Available online at www.sciencedirect.com
SCIENCE DIRECT®
Estuarine, Coastal and Shelf Science 63 (2005) 57–72
ESTUARINE COASTAL AND SHELF SCIENCE
www.elsevier.com/locate/ECSS

Optical water quality of a blackwater river estuary: the Lower St. Johns River, Florida, USA

Charles L. Gallegos

Smithsonian Environmental Research Center, P. O. Box 28, Edgewater, MD 21037, USA

Received 12 August 2004; accepted 18 October 2004

Abstract

This paper reports measurements of absorption and scattering coefficients in relation to standard water quality measurements in the St. Johns River (Florida, USA), a blackwater river in which phytoplankton chlorophyll and non-algal particulates as well as colored dissolved organic matter (CDOM) contribute substantially to the inherent optical properties of the water. Extremely high concentrations of CDOM in this river present special problems for the measurement of inherent optical properties, such as the presence of very fine particulate matter that passes through most glass fiber filters. Empirical relationships are presented for estimating true dissolved absorption at very high CDOM concentrations. Specific-absorption and -scattering coefficients of suspended particulate matter varied widely, but appeared to decline steadily with salinity at salinities above 5, consistent with increasing influence of large-sized, unconsolidated mineral particulates with increasing tidal energy near the estuary mouth. Relationships are given for prediction of inherent optical properties from water quality concentrations for use in radiative transfer modeling, and changes in water quality measurements are recommended that can avoid the need for empirical corrections.

Keywords: St. Johns River; estuaries; optical properties; light penetration; water quality; colored dissolved organic matter; chlorophyll; total suspended solids

1. Introduction

Light penetration is of fundamental importance to aquatic systems for a variety of reasons. Primary production by phytoplankton is a light dependent process that provides the energy to drive plankton and microbial food webs that typically takes place down to depths to which about 1% of surface light penetrates (i.e. the euphotic zone). Submerged vascular plants require considerably greater amounts of light than phytoplankton, on the order of 13–37% of surface irradiance (Dennison et al., 1993). Indeed, reduction of light penetration associated with over enrichment of estuaries by anthropogenic nutrient loading leading to eutrophication is one of the primary causes of loss of submerged aquatic vegetation (Kemp et al., 1983). Similarly, underwater image propagation affects the success of visually orienting predatory fish, so that optical properties have been suggested as a top–down influence on marine pelagic food webs through their control on fish predation (Aksnes et al., 2004).

Human perception of the aesthetic and recreational value of a water body is also closely associated with optical properties and light penetration (Davies-Colley et al., 1993). An annual activity in the Chesapeake Bay region involves public ''wade-in''s, in which citizen groups wade into certain tributaries until they can no longer see their toes, as an index of the progress of Bay cleanup efforts (see, e.g. http://www.dnr.state.md.us/bay/tribstrat/wadein_results.html). Such events raise public awareness and involvement in water quality issues, and at the same time, place pressure on managers

E-mail address: gallegosc@si.edu

0272-7714/$ - see front matter © 2004 Elsevier Ltd. All rights reserved.
doi:10.1016/j.ecss.2004.10.010

and planners to make the water quality improvements needed to improve water clarity.

Management activities aimed at improving water clarity in estuaries must reduce concentrations of the dissolved and suspended materials that absorb and scatter light. The optically significant components are colored dissolved organic matter (CDOM), phytoplankton chlorophyll *a* (CHLA), and non-algal particulates (NAP). In estuaries, all of these light attenuating components of the water may occur in appreciable amounts. Due to the influence of freshwater discharge and resuspension of bottom sediments by physical processes in estuaries, the concentrations of these components generally do not bear any simple relationship with one another. Determining the amount of reduction needed of various light attenuating components is a problem for modeling light behavior in water. When the inherent optical properties of the water are known, the propagation of light under water can be calculated by a variety of radiative transfer schemes available (Mobley et al., 1993).

Instruments for measuring inherent optical properties, i.e. the absorption, scattering, and backscattering coefficients, of the water column are now widely available in the research community. However, such instruments have not been in use so long as to acquire long time series (i.e. several years) of repetitive measurements in any single location. In some areas, programs have been in place for many years to measure water quality parameters that, though ill defined in terms of true inherent optical properties, nevertheless depend in some way on the optical properties. For example, the visual comparison test for measuring color of natural water, which involves making a visual match between a filtered sample and serial dilutions of a stock Pt-Co solution in nessler tubes, depends on the qualitatively similar absorption spectrum of CDOM and the Pt-Co solution at visible wavelengths (Cuthbert and del Giorgio, 1992). In spite of inherent limitations, it is desirable to have the capability to use such measurements in estuaries to reveal causes of light attenuation, sources of light attenuating components, and long-term trends in water clarity. To use water quality measurements in this way requires knowledge of the relationships between inherent optical properties and the relevant water quality measurement. Inherent optical properties have the desirable characteristic that their value is proportional to the concentrations of the causative factors (Kirk, 1994). The proportionality constants between absorption or scattering coefficients and a water quality measure are termed specific-absorption and specific-scattering coefficients. The specific-absorption and -scattering coefficients of materials depend on qualitative features of the component. For example, the specific-absorption coefficient of CHLA depends on the size, shape, and pigmentation of phytoplankton populations (Bricaud et al., 1988; Stramski et al., 2001), and the specific-scattering coefficient of mineral particulates depends on the particle-size distribution, index of refraction, and specific-gravity (Babin et al., 2003a; Wozniak and Stramski, 2004).

The relationships between optical properties and commonly measured water quality parameters have received some attention. For example, the visual color test has been shown to be a predictor of the absorption spectrum by CDOM (Bowling et al., 1986; Gallegos and Kenworthy, 1996), though the proportionality constant between visual color on the Pt-Co scale and CDOM absorption at a specified wavelength varies regionally (Cuthbert and del Giorgio, 1992). Similarly, Wells and Kim (1991) found that the scattering coefficient was sometimes well correlated with measurements of total suspended solids (TSS) for limited time periods in the Neuse River, North Carolina (USA), though no correlation was observed for seasonal time scales.

The objective of this work was to develop relationships between inherent optical properties and routinely measured water quality variables for the Lower St. Johns River, Florida (USA) that can be used as input for radiative transfer modeling in this optically complex system. The St. Johns River is a blackwater estuary on the east coast of Florida, in which CDOM, CHLA, and NAP all occur in appreciable quantities. The overall variability in specific-absorption and -scattering coefficients was examined along a gradient of stations from tidal fresh to the sea, and over two different time periods characterized by historically dry (1999–2000) and more normal rainfall (2003). Results indicate that linear relationships between inherent optical properties and routinely measured water quality parameters break down at the extremely high CDOM concentrations that typify this system, presenting interesting challenges for optical analysis.

2. Study site

The St. Johns River is a northward flowing, blackwater river in northeast Florida (USA). The river originates in floodplains north of Lake Okeechobee, from which it derives much of its CDOM. The lower St. Johns River (LSJR), which extends from the confluence of the Ocklawaha River to its mouth at the Atlantic Ocean east of Jacksonville, is broad and shallow, averaging about 3 m depth. The LSJR is tidal throughout its length, with an amplitude of about 1.4 m at the mouth, decreasing irregularly upstream due to changes in channel morphology (Morris, 1995).

Samples were collected during two time periods: approximately quarterly during 1999 and 2000, and monthly for 10 months from March 2003 to January 2004. The first period was near the end of an extended drought, during which color measurements were at the low end of the historically measured range. The second sampling period, which was needed to obtain samples from the full range of

expected CDOM concentrations, occurred after the resumption of more normal rainfall patterns.

During the first sampling period we occupied a series of stations from Crescent Lake to the mouth of the St. Johns River at Mayport, Florida (Fig. 1, open and filled circles). The sampling objective during this phase was to obtain samples from the widest gradient in optical properties obtainable, thereby characterizing salt and freshwater end members, and the gradient of mixtures in between. During the second phase, samples were collected by personnel of the St. Johns River Water Management District (SJRWMD) and shipped to the Smithsonian Environmental Research Center (SERC, Edgewater, Maryland) for analysis. Sampling sites during the second phase, some of which coincided with those of the first phase (Fig. 1, squares and filled circles), were chosen among high-color sites regularly visited in ongoing water quality monitoring programs of the SJRWMD. Phase 2 sampling included the effluent from a retention impoundment of a Georgia Pacific pulp processing facility.

3. Inherent optical properties and water quality measurements

3.1. Absorption

Light absorption by different components is additive, proportional to the concentration of the causal agent,

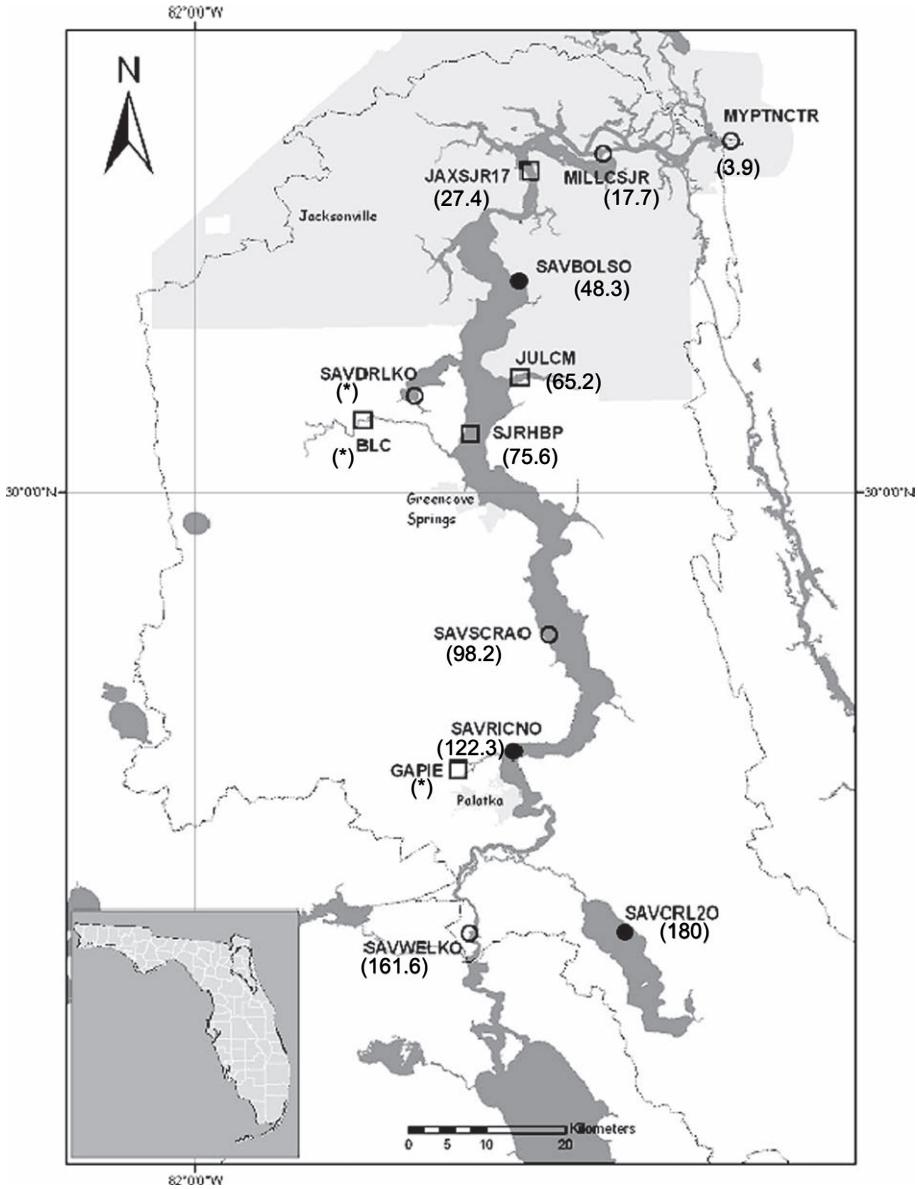

Fig. 1. Map of Lower St. Johns River showing locations of stations sampled during the relatively dry period 1999–2000 (open circles), during the period of normal rainfall 2003–2004 (open squares), and during both periods (filled circles). Numbers in parentheses are distance from the mouth (km). Stations off the main channel axis (*) were not included in spatial plots. Inset shows location of the Lower St. Johns River in northeast Florida (USA).

and a function of wavelength, λ. Therefore, we can write the total absorption as the sum of absorption spectra:

$$a_t(\lambda) = a_w(\lambda) + a_g(\lambda) + a_\phi(\lambda) + a_{p-\phi}(\lambda) \quad (1)$$

where a = absorption coefficients and the subscripts t, w, g, ϕ, and $p-\phi$, stand for, respectively, total, water, CDOM (i.e. *gelbstoff*, Kirk, 1994), phytoplankton, and non-algal particulates. The representation of the spectral variability is simplified by defining normalized absorption spectra for the water quality constituents as the absorption at wavelength λ divided by the absorption at some reference wavelength, λ_r. By convention (Kirk, 1994) 440 nm is used as a reference wavelength for CDOM and NAP absorption, and 676 nm for chlorophyll because it is an absorption peak that is distinctly different from other components. Additionally, it is convenient to reference total absorption to absorption by water, since that is how available instrumentation measures it. That is:

$$a_{t-w}(\lambda) = a_g(440)g(\lambda) + a_\phi(676)\phi(\lambda) + a_{p-\phi}(440)p(\lambda) \quad (2)$$

where a_{t-w} is the total absorption less than that due to pure water, and the functions $g(\lambda)$, $\phi(\lambda)$, and $p(\lambda)$ are absorption spectra due to, respectively, CDOM, phytoplankton, and non-algal particulates normalized to the stated reference wavelengths.

Absorption by CDOM has been shown to vary with wavelength as a negative exponential, which in the visible spectrum, can be described using a single spectral slope (e.g., Bricaud et al., 1981). The normalized absorption function for CDOM can be written as:

$$g(\lambda) = \exp\left[-s_g(\lambda - 440)\right] \quad (3)$$

where s_g is the exponential slope of absorption by CDOM. The normalized absorption spectrum of NAP has a similar exponential shape (Roesler et al., 1989), but with a different, generally smaller, value for spectral slope, denoted here as s_p, and again, a reference wavelength of 440 nm is used. The normalized absorption spectrum of phytoplankton does not have a convenient analytical expression, and is generally presented as tabulated values.

The final step in relating the absorption spectrum to standard water quality measurements is to determine the scaling between the absorption coefficient at the reference wavelength and water quality concentration. The scale factor relating absorption at a reference wavelength to the water quality measurement is called the specific-absorption coefficient. We can then write:

$$a_{t-w}(\lambda) = a_g^*(440)[\text{Color}]g(\lambda) + a_\phi^*(676)[\text{CHLA}]\phi(\lambda) + a_{p-\phi}^*(440)[\text{TSS}]p(\lambda) \quad (4)$$

where coefficients with asterisks are specific-absorption coefficients at the reference wavelength in parentheses, and water quality measurements are Color by the visual comparison method for CDOM, (CHLA) for chlorophyll in phytoplankton, and (TSS) for non-algal particulates.

To determine the normalized absorption spectra and the specific-absorption coefficients, the different constituents can be separated and their absorption spectra measured in the laboratory (see Section 4). The normalized absorption spectra are not constant, but are generally less variable than the water quality concentrations themselves. Ideally the relationship between absorption and the relevant water quality measurement would be linear, but qualitative changes in the material measured by the standard water quality measurement, for example, size and species composition of phytoplankton, or size distribution and mineralogy of the particulate matter, can create variability in both the specific-absorption coefficients and spectral shapes. In the subsequent analysis, I fit linear relationships and use the slope as the specific-absorption coefficient when successful, and otherwise report the distribution of the specific-absorption coefficient determined from the ensemble of measurements, $a_x(\lambda_r)/C_x$, where C_x is the concentration of absorption component x.

3.2. Scattering

Scattering by particulate matter was treated in a similar manner as absorption. That is, the spectral shape of particulate scattering was defined by a normalized scattering function, $b_n(\lambda)$, and the scattering spectrum was represented as:

$$b_p(\lambda) = b_p(555)b_n(\lambda) \quad (5)$$

where $b_p(\lambda)$ is the scattering coefficient at wavelength λ, and $b_p(555)$ is to be predicted from the concentrations of water quality constituents. 555 nm was chosen as the reference wavelength because it is a minimum within the visible range in particle absorption (Babin et al., 2003a). As with absorption, all particulate matter in a sample, living and non-living, contributes to scattering, and each type of material could have its own normalized scattering function. Unlike absorption, however, the different types of particulate matter cannot be separated from one another in the process of measuring scattering coefficient. In principle, the shape of the scattering spectrum can be calculated by Mie theory (Babin et al., 2003a,b), but to do so it requires information on particle-size spectra and refractive index that is generally not available in routine water quality monitoring programs. In keeping with the objectives of this paper, I analyzed the shapes of the measured $b_n(\lambda)$ solely in

terms of measured water quality variables, TSS, CHLA, and CDOM.

4. Methods

In the laboratory I measured absorption, $a_{t-w}(\lambda)$, and beam attenuation coefficients, $c_{t-w}(\lambda)$, of water samples at nine wavelengths in the visible range using WETLabs ac-9 absorption-attenuation meter with 10 cm flow tube, at wavelengths 412, 440, 488, 510, 532, 555, 650, 676, and 715 nm. To avoid bubble entrainment, water was gravity-fed through the instrument at a flow rate of about 1.5 l min^{-1}, and data logged using the manufacturer's Wetview software. Temperature- and salinity-corrected absorption coefficients were corrected for scattering as described by Gallegos and Neale (2002). Particulate scattering, $b_p(\lambda)$, was calculated from the difference, $b_p(\lambda) = c_{t-w}(\lambda) - a_{t-w}(\lambda)$. Whenever $c_{t-w}(412)$ was >30 m^{-1}, samples were diluted 1:2 serially until measurements fell below that limit to keep samples within the manufacturer's stated sensitivity (adjusted to 10 cm flow path). Final coefficients were scaled by the appropriate dilution factor.

I measured absorption by CDOM on water filtered through a 0.22 μm pore-diameter polycarbonate membrane filter (Poretics) using 5-cm pathlength quartz cells referenced to a similarly filtered distilled water blank in a Cary dual beam spectrophotometer. Measurements in absorbance units (AU) were converted to in situ absorption coefficients, $a_{\mathrm{CDOM}}(\lambda)$, by multiplying by 2.303 [i.e. ln(10)] and dividing by the pathlength, 0.05 m.

I measured absorption by particulate matter, $a_{\mathrm{p}}(\lambda)$, using the quantitative filter pad technique (Kishino et al., 1985). A volume of water was filtered onto a 25 mm glass fiber filter (Whatman GF/F) and frozen (−20 °C) for <4 weeks. For measurements, filters were thawed and re-wetted with 200 μL of filtered distilled water and placed next to the exit window of the sample beam of the Cary spectrophotometer. Absorbance was measured relative to a moistened blank GF/F filter placed next to the exit window of the reference beam. Measured absorbances were converted into in situ particulate absorption coefficients multiplying by 2.303 and dividing by the geometric pathlength (= volume filtered/area of filter), and division by a pathlength amplification factor, $\beta = 1.5$ (Tzortziou, 2004), determined by comparing filterpad measurements with measurements made on a solution contained inside an integrating sphere (Babin and Stramski, 2002). On one occasion, I measured absorption by fine particulate matter that passed a GF/F filter, but was caught on a 0.22 μm polycarbonate membrane filter. The membrane filter was placed on a moistened backing GF/F filter, and read as above against a similar membrane-GF/F combination reference.

For determination of chlorophyll concentrations, whole-water samples were filtered onto GF/F filters, and stored frozen up to 4 weeks. Filters were thawed and extracted in 90% acetone overnight at 4 °C in the dark. Chlorophyll concentrations, uncorrected for phaeopigments, were calculated from spectrophotometric absorbance measurements by the equations of Jeffrey and Humphrey (1975). Turbidity (NTU) was measured using a Hach 2100N turbidimeter. The concentration of TSS was measured from the weight gain of a pre-rinsed, pre-combusted (525 °C, 2 h) GF/F glass fiber filter, divided by the volume filtered.

5. Results

5.1. CDOM and visually determined color

Salinity was a poor overall predictor of CDOM absorption at 440 nm within each sampling period and within most individual sampling dates, due to large spatial variations within the tidal freshwater reach (Fig. 2). There was generally a linear relationship between salinity and $a_g(440)$ on individual cruises only down estuary of the most seaward fresh station (examples in Fig. 2a,b connected points). The location of the most seaward fresh station varied with flow conditions, but was always further up estuary in the first sampling period than during the second, more rainy period. Salinity was always <1 upriver of 100 km, yet variations in $a_g(440)$ in that region were large during both periods (Fig. 2b,c). During the first (dryer) sampling period, there was often an increase in $a_g(440)$ at Rice Creek (Fig. 2c, station SAVRICNO, 122 km), the creek that receives the effluent from the Georgia Pacific paper mill. No such increase at station SAVRICNO was observed during the wetter sampling period (Fig. 2d), but instead there was occasionally an increase in $a_g(440)$ at Julington Creek (Fig. 2d, JULCM, 65 km). Overall, CDOM absorption was up to twofold higher during the wet period than during the dry sampling period (cf. Fig. 2c,d).

The spectral slope of absorption by CDOM varied from 0.0135 to 0.0220 nm^{-1}, with an average of 0.0157 nm^{-1} in samples from the river, and was as low as 0.0107 nm^{-1} in samples from the Georgia Pacific impoundment effluent (GAPIE). The spectral slope is known to depend on the composition of the organic matter (Carder et al., 1989), and to increase as the CDOM undergoes photobleaching (Vodacek et al., 1997). The s_g parameter showed a high degree of variability at tidal freshwater stations, and varied only weakly at salinities greater than 5 (Fig. 3a). At salinities less than 15 there was no significant difference

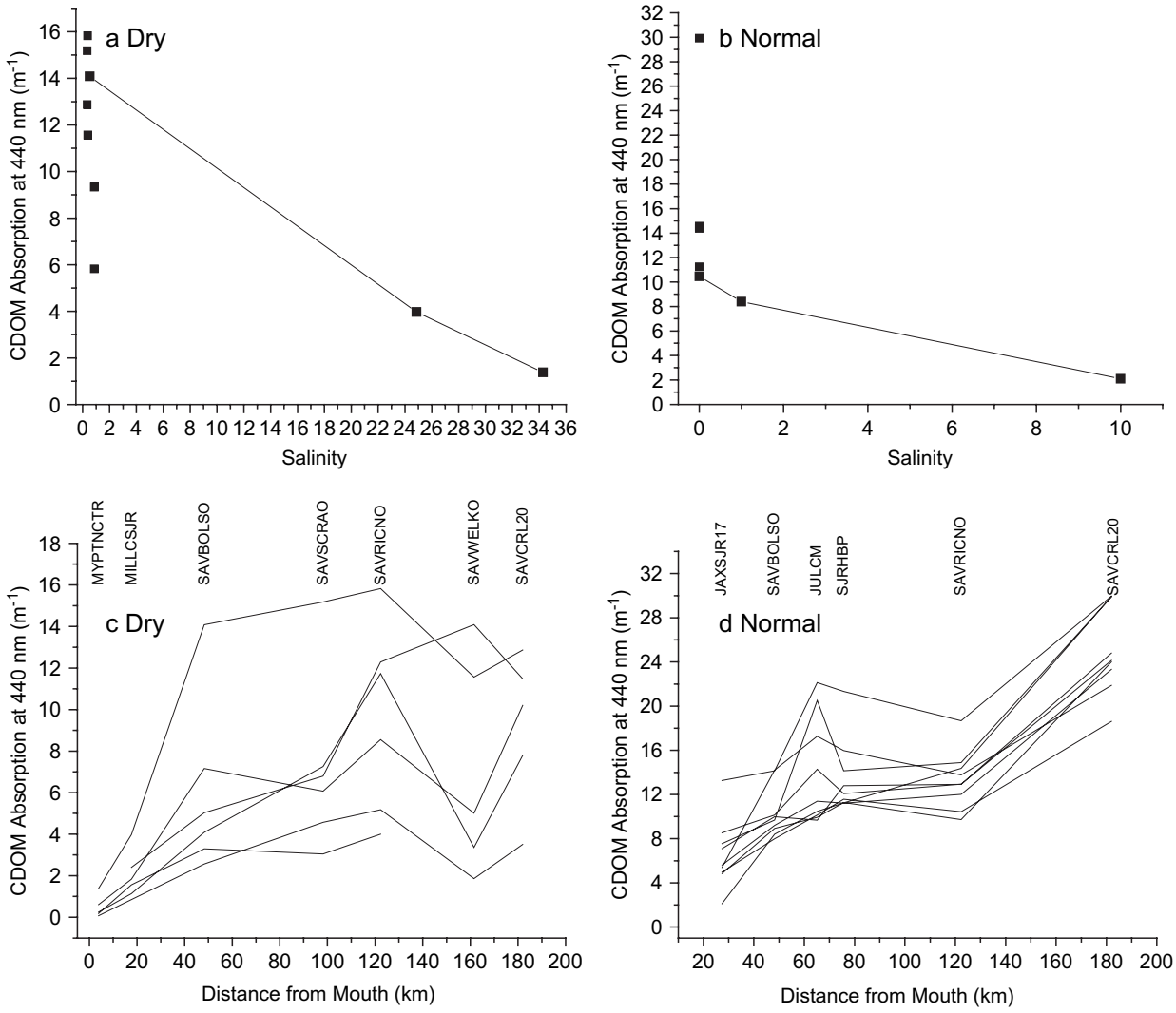

Fig. 2. (a,b) Absorption by colored dissolved organic matter (CDOM) at 440 nm plotted against salinity on a single cruise during (a) the dry sampling period and (b) the period of normal rainfall. Solid lines connect the three most seaward stations. Both sampling periods show substantial variation in CDOM absorption within the tidal fresh region (i.e. at 0 salinity). (c,d) CDOM absorption at 440 nm plotted against distance from mouth during (c) the dry sampling period, and (d) the period of normal rainfall. Station names above plots are for reference (cf. Fig. 1).

($P = 0.09$) in s_g between the dry and wet sampling periods among river samples (i.e. excluding GAPIE). Spatial trends were similarly weak, with s_g showing a slight trend toward higher values seaward of about 60 km (Fig. 3b). The s_g parameter bore the strongest relationship with CDOM absorption itself (Fig. 3c).

Color concentrations at river stations measured by the visual comparison test ranged from 10 to 250 Pt units during 1999–2000, but were higher on average ranging up to 500 Pt units in 2003 (Fig. 4a). The relationship between CDOM absorption measured spectrophotometrically and color measured visually appeared nonlinear, with a steeper slope at color less than 100 Pt units (Fig. 4a). There is, however, a difference in filters used between visual color determination, which uses Whatman GF/C glass fiber filters with a nominal pore diameter of 1.2 μm, and spectrophotometric measurement of CDOM absorption, which uses 0.22 μm polycarbonate membrane filters. On one sampling date in June 2003, color was determined by the visual comparison method after filtering through GF/C filters and again after filtering through 0.22 μm polycarbonate membrane filters (Fig. 4b). At color concentrations above 200 Pt units color measured after filtration through 0.22 μm filters was less than that measured after filtering through GF/C filters, and was only half the reading at the highest color concentration, measured at the GAPIE station (Fig. 4b).

Thus, at high CDOM concentrations there is fine particulate matter that passes through a 1.2 μm glass fiber filter that is removed by a 0.22 μm membrane filter. When filters of the same pore diameter (i.e. 0.22 μm) were used for both tests, the relationship remained linear to color concentrations of 800 Pt units, or CDOM absorption at 440 nm of 55 m^{-1} (Fig. 4c). Thus it

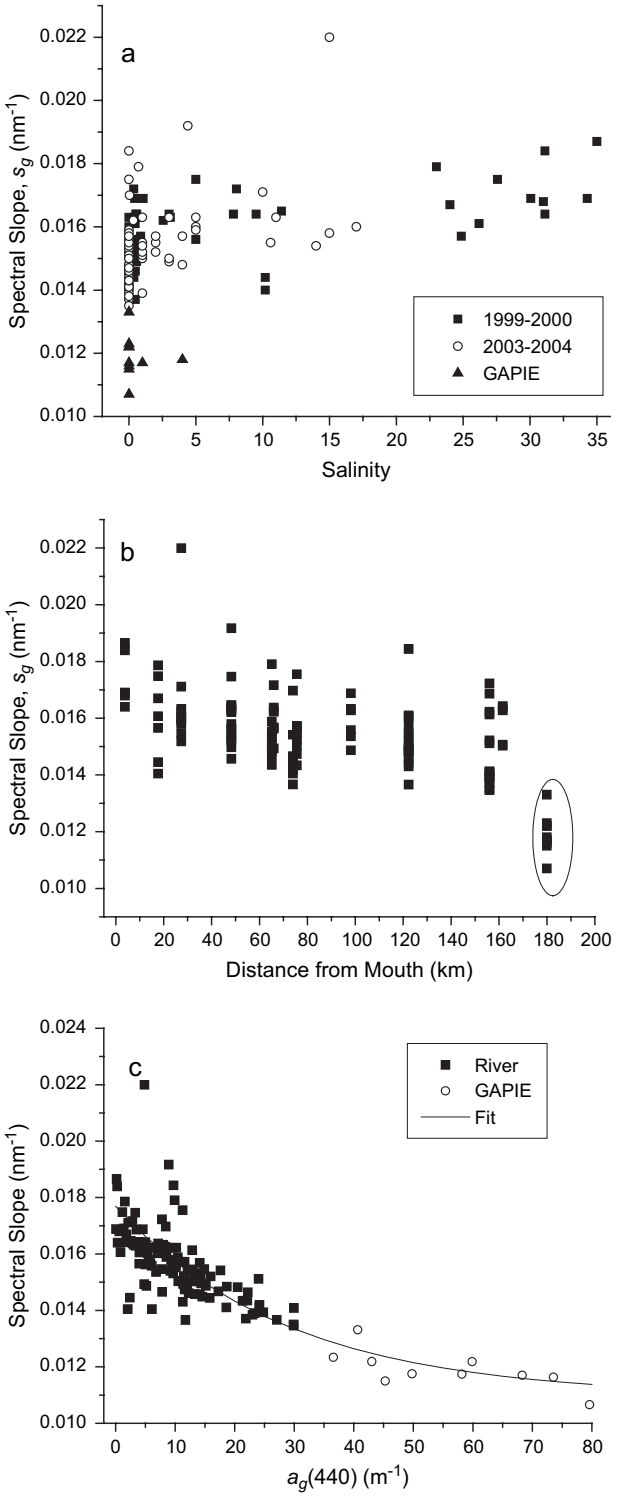

Fig. 3. (a) Spectral slope of CDOM absorption, s_g, plotted against salinity, which included higher values during the dry period (filled squares, 1999–2000) than during the wet period (open circles, 2003–2004). (b) s_g plotted against distance from mouth. Samples from the Georgia Pacific impoundment effluent (GAPIE, encircled points in (b)) were arbitrarily plotted at 180 km. (c) s_g plotted against CDOM absorption at 440 nm. CDOM absorption was the best predictor of s_g (see Eq. (7)), indicated by solid line. Samples from GAPIE (open circles) constrain the fit at high CDOM concentrations, though values that were high were not encountered at river stations.

appears that the fine particulate material is responsible for the nonlinear relationship between measured CDOM absorption and visually determined color (Fig. 4a). Shipment of the sample from Florida to Maryland only resulted in loss of CDOM at the highest concentration, in the sample from the GAPIE station (Fig. 4d).

In summary, to estimate absorption by CDOM from visually determined color in Pt units in the St. Johns River, it is necessary to correct visual color estimates above 200 Pt units for contribution of fine particulates. I found this correction to be fit by an empirical power formula given by:

$$\mathrm{Color_{diss}} = 200\left(\frac{\mathrm{Color_{meas}}}{200}\right)^{0.665} \quad (\mathrm{Color_{meas}} > 200) \qquad (6a)$$

and

$$\mathrm{Color_{diss}} = \mathrm{Color_{meas}} \quad (\mathrm{Color_{meas}} \leq 200) \qquad (6b)$$

where $\mathrm{Color_{diss}}$ = color measured visually on 0.22 μm-filtered water, $\mathrm{Color_{meas}}$ = color measured on GF/C-filtered water, and the constants are specified for continuity at $\mathrm{Color_{meas}}$ = 200 Pt units. The proportionality between $a_g(440)$ and $\mathrm{Color_{diss}}$ (i.e. $a_g^*(440)$) was found to be 0.065 m^{-1} (Pt units)$^{-1}$. That is:

$$a_g(440) = 0.065\,\mathrm{Color_{diss}} \qquad (6c)$$

The data in Fig. 3c were fit by an exponential approach to an asymptote:

$$s_g = 0.011 + 0.00764\exp\left[-0.0346 a_g(440)\right] \qquad (7)$$

completing the evaluation of parameters needed to specify the absorption due to CDOM in Eq. (4).

5.2. Chlorophyll

The concentration of chlorophyll measured by SERC personnel agreed well with that measured by the Water Management District whether the measurements were made on site (Fig. 5a, filled squares) or shipped to Maryland (Fig. 5a, open circles). However, there was apparently an effect of very high CDOM on determination of the normalized chlorophyll absorption that was seen as unrealistically high values at blue wavelengths, e.g. $\phi(440)$ (Fig. 5b). Values in excess of 4 (dimensionless) were measured at CDOM concentrations as low as 1 m^{-1} when CHLA < 10 mg m^{-3} (Fig. 5b, open circles), and at CDOM concentrations >13 m^{-1} when CHLA > 10 mg m^{-3} (Fig. 5b, filled squares). This could occur if the methanol extraction procedure to remove phytoplankton pigments also extracted particulate color from non-algal particulate matter. Not every sample meeting those criteria showed the effect, but it occurred often enough to adversely affect the determination of $\phi(\lambda)$. For determination of the averaged $\phi(\lambda)$ therefore, I

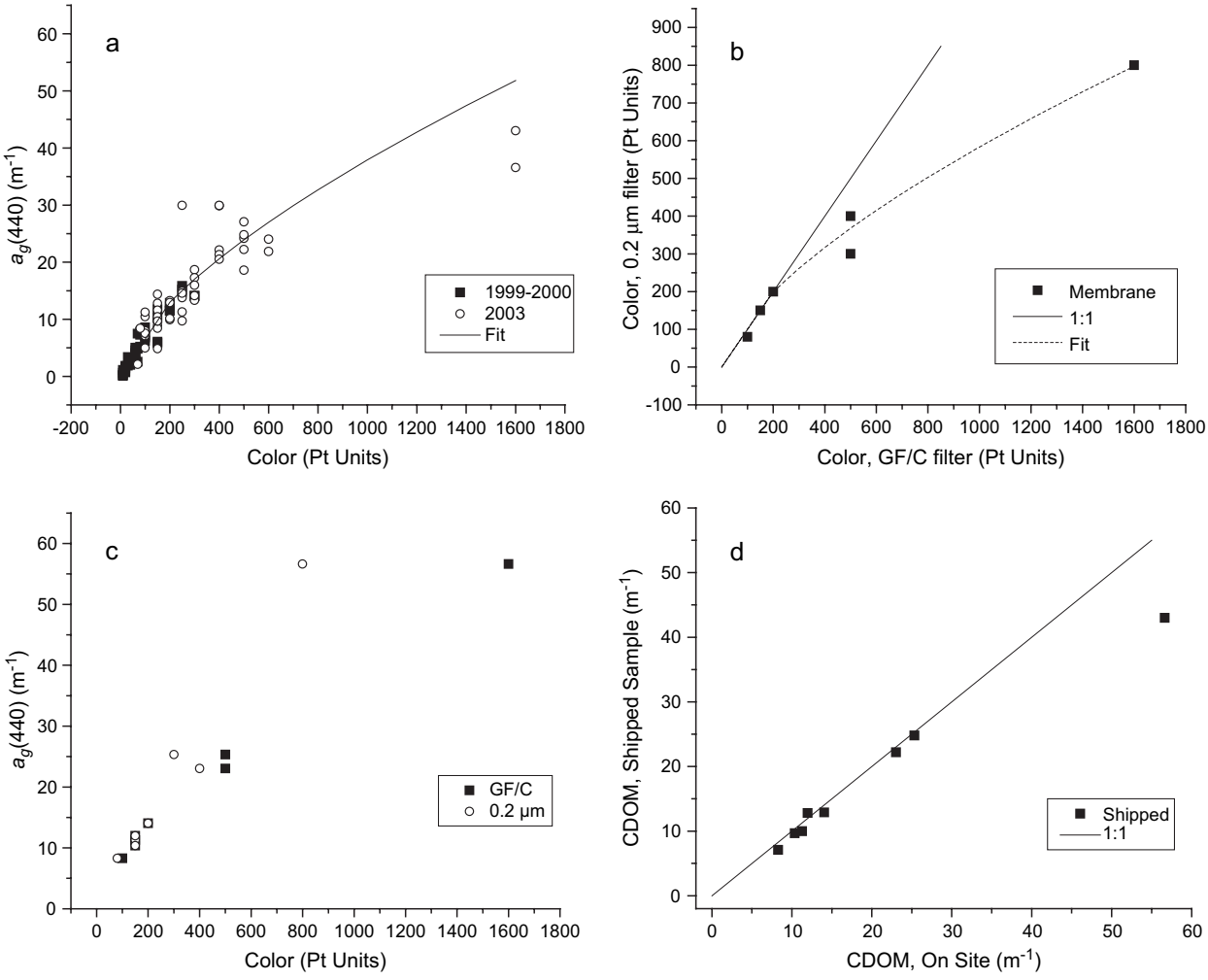

Fig. 4. (a) Absorption by CDOM at 440 nm, $a_g(440)$, plotted against visually estimated color during the (filled squares) dry period and (open circles) wet period. Solid line is power-function fit. (b) Visually estimated color concentration on sample filtered through 0.2 µm filter against visually estimated color estimated on sample filtered through GF/C glass fiber filter. Solid line is line of equality; dashed line is fit of Eq. (6a)–(6c). (c) $a_g(440)$ against visually estimated color after filtration through (filled squares) GF/C glass fiber filter, and (open circles) 0.2 µm membrane filter. Membrane filtration maintained linearity to $a_g(440) = 55\ \mathrm{m}^{-1}$, or 800 Pt units. (d) CDOM absorption at 440 nm after shipment to Maryland against absorption measured prior to shipment in Florida. Only the sample from GAPIE (55 m^{-1}) experienced appreciable loss of CDOM.

restricted measurements to samples high in CHLA and low in CDOM satisfying the two simultaneous criteria CHLA $> 10\ \mathrm{mg\,m}^{-3}$ and $a_g(440) < 13\ \mathrm{m}^{-1}$. The resulting averaged normalized chlorophyll absorption spectrum was unremarkable in shape (Fig. 5c) and showed a typical amount of sample-to-sample variability for studies of this kind (e.g. Bricaud et al., 1995). Phytoplankton absorption at 676 nm varied linearly with chlorophyll with no difference between sampling periods (Fig. 5d). The specific-absorption coefficient for phytoplankton chlorophyll at 676 nm was $0.0185\ \mathrm{m}^2$ $(\mathrm{mg\ CHLA})^{-1}$.

5.3. Non-algal particulates

Absorption by NAP varied with wavelength according to a negative exponential, with an average spectral slope, s_p, of $0.00853\ \mathrm{nm}^{-1}$, ranging from 0.0049 to $0.0151\ \mathrm{nm}^{-1}$. Unlike s_g, s_p did not vary systematically with salinity, distance from the mouth, or the overall magnitude of $a_{p-\phi}(440)$. However, s_p did vary significantly between the sampling periods ($F = 34.5$, $P < 0.001$), averaging $0.00776\ \mathrm{nm}^{-1}$ during the dryer 1999–2000 sampling period, and $0.00905\ \mathrm{nm}^{-1}$ during 2003–2004.

Relating absorption by NAP at a reference wavelength (440 nm) to water quality measurements was complicated by methodological difficulties. Total suspended solids is an inherently noisy measurement because it involves subtraction of two filter weights, so that agreement between labs was not as strong as that for chlorophyll (Fig. 6a). Most of the TSS measurements fell within $\pm 15\ \mathrm{g\,m}^{-3}$ of one another, but 10 samples did not, and these were excluded from the

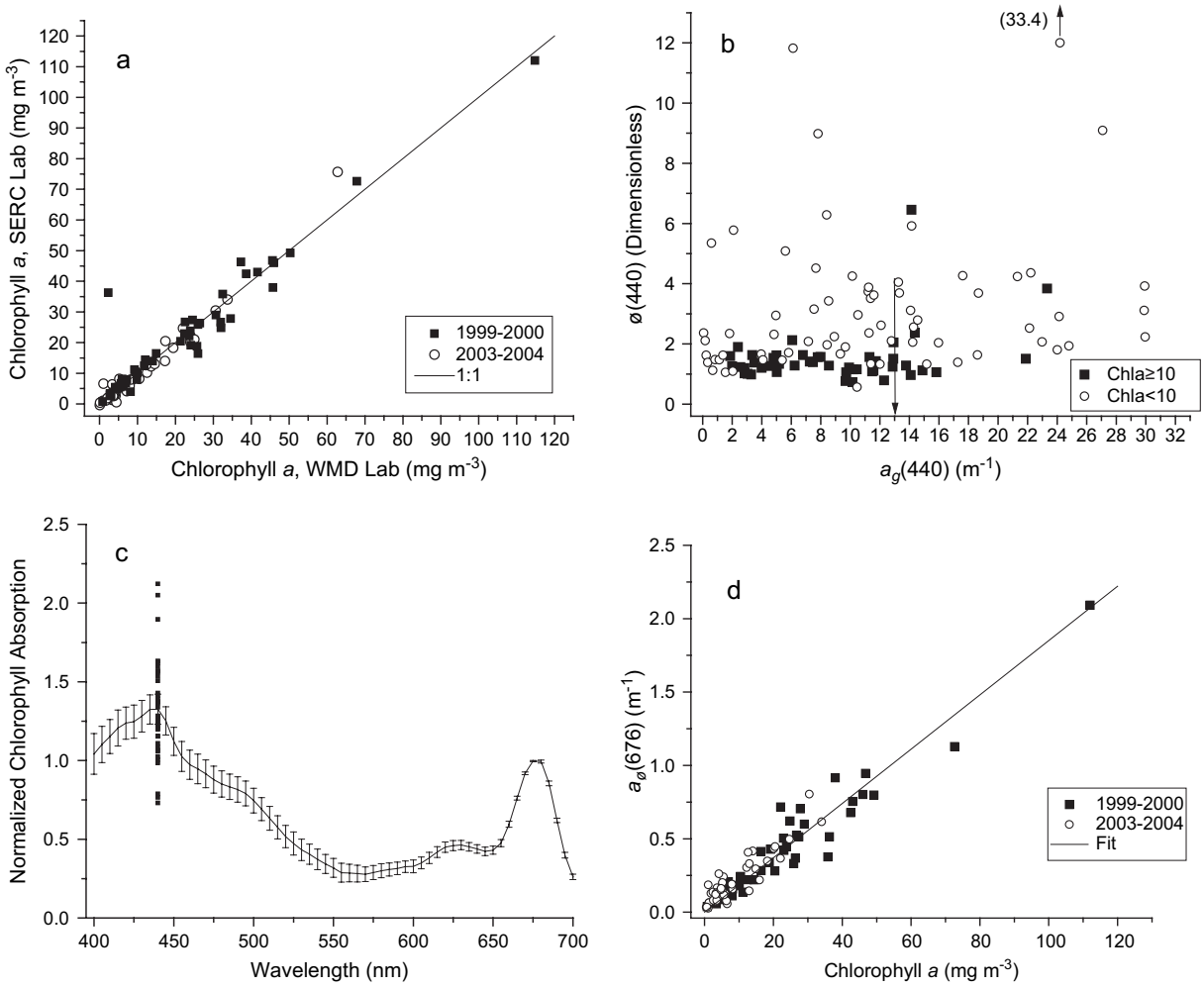

Fig. 5. (a) Inter-laboratory comparison of chlorophyll analyses on samples from (filled squares) the dry period (1999–2000) and (open circles) the wet period (2003–2004). Analyses by the SERC lab during the wet period done after shipment of the samples from Florida to Maryland. (b) Normalized absorption by phytoplankton chlorophyll plotted against CDOM absorption at 440 nm, $a_g(440)$ for samples with (filled squares) chlorophyll greater than 10 mg m^{-3} and (open circles) chlorophyll less than 10 mg m^{-3}. Arrow at $a_g(440) = 13$ m^{-1} indicates cutoff above which samples were rejected for determination of normalized absorption function (see text). (c) Ensemble average (solid line) of phytoplankton absorption spectrum normalized to absorption at 676 nm. Error bars are ± 2 standard errors of the mean. Filled squares are all observations at 440 nm. (d) Absorption by phytoplankton at 676 nm, $a_\phi(676)$, plotted against chlorophyll concentration for (filled squares) dry sampling period 1999–2000, and (open circles) wet sampling period 2003–2004. Solid line is linear fit with specific-absorption coefficient, $a^*_\phi(676) = 0.0185$ m^2 (mg Chl a)$^{-1}$.

analysis. Nearly all the samples from GAPIE were eliminated for this reason, having much higher values for TSS after shipment (Fig. 6a).

The relationship between $a_{p-\phi}(440)$ and TSS appeared depend on salinity (Fig. 6b). The transition zone in the LSJR is abrupt, which led to breaks in the sampled salinity distribution, i.e. no samples were obtained with salinities falling between 5 and 7.5, or between 15 and 20. Samples from tidal freshwater and oligohaline stations (salinity, $S \leq 5$) had a higher specific-absorption coefficient (Fig. 6b, filled squares) than for samples with salinity in the middle range ($7.5 \leq S \leq 15$, Fig. 6b, open circles) which were higher still than those collected seaward of the estuarine mixing zone (Fig. 6b, filled triangles). Additionally, there were several outliers among samples from tidal freshwater stations that fell well above the overall scatter of points (Fig. 6b, encircled points). Plotted against turbidity as an alternate measure of particle concentration, these seven points were near the upper range of the overall spread of points, but not obvious outliers (Fig. 6c, open triangles). Thus in the case of the outliers from low-salinity stations, it is reasonable to suspect random underestimation of TSS in these few cases. For the samples from the middle and high salinity ranges, there could be either systematic overestimation of TSS, or genuine differences in both the absorption per unit mass and turbidity per unit mass in particulate matter from stations within and seaward of the estuarine mixing zone. Because of the overall degree of scatter in the relationships, I plotted the frequency distribution of specific-absorption coefficient for NAP for individual

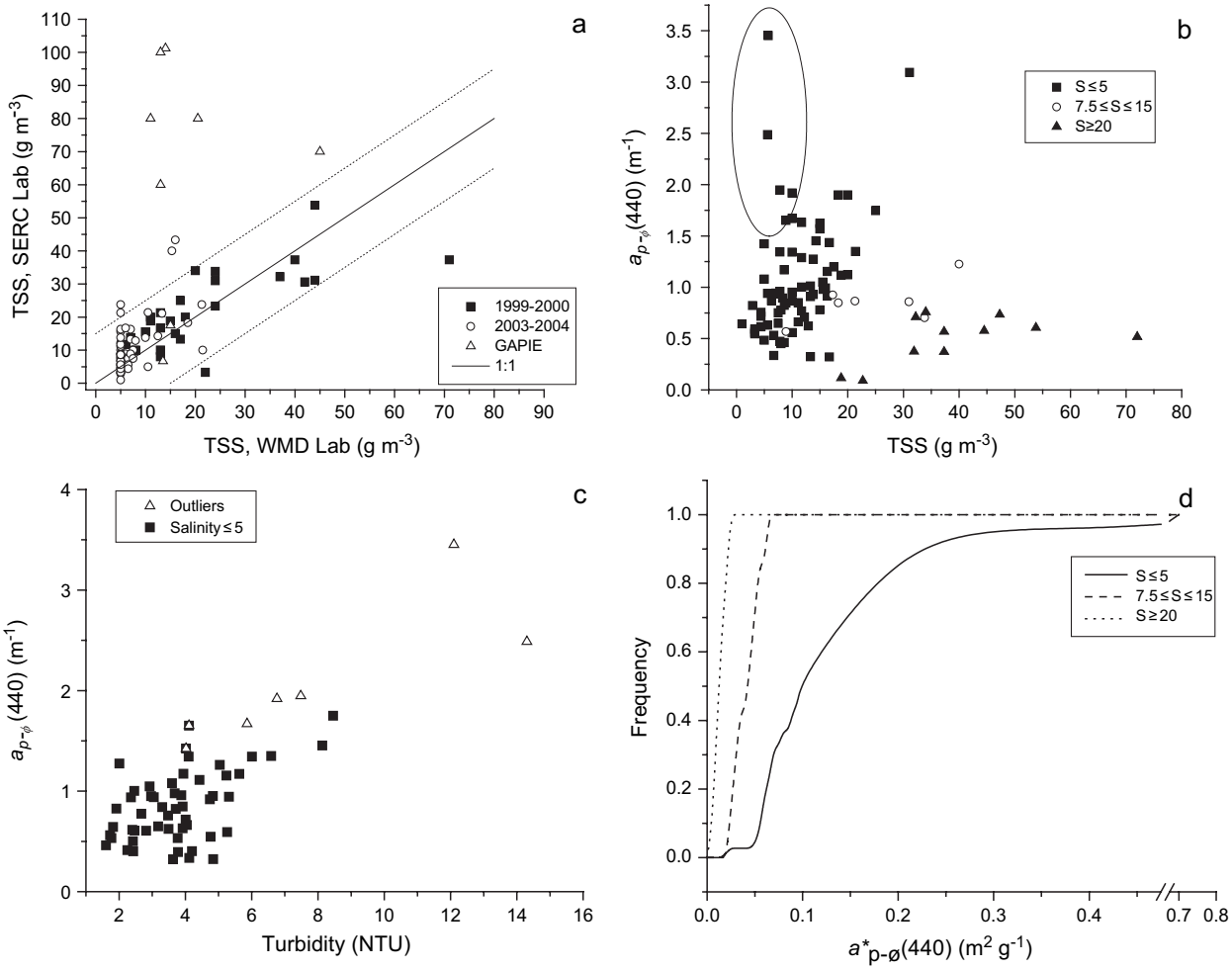

Fig. 6. (a) Inter-laboratory comparison of total suspended solids (TSS) analyses on samples from (filled squares) the dry period (1999–2000) and (open circles) the wet period (2003–2004). Analyses by the SERC lab during the wet period were done after shipment of samples from Florida to Maryland. Solid line is line of 1:1 agreement. Analyses that differed by more than ± 15 g m^{-3} (dotted lines), including all samples from the GAPIE station (open triangles) were eliminated from analysis for specific-absorption and -scattering coefficients. (b) Absorption by non-algal particulate matter at 440 nm, $a_{p-\phi}(440)$ plotted against TSS for samples with (filled squares) salinity (S) ≤ 5, $7.5 \leq S \leq 15$ (open circles) and (filled triangles) $S \geq 20$. (c) Encircled outliers from low-salinity samples (open triangles) were indistinguishable when $a_{p-\phi}(440)$ was plotted against turbidity. (d) Cumulative frequency distributions of specific-absorption coefficient calculated for individual samples as $a_{p-\phi}(440)$/TSS for samples with salinity (S) ≤ 5 (solid line), $7.5 \leq S \leq 15$ (dashed line) and $S \geq 20$ (dotted line).

samples estimated as $a_{p-\phi}(440)$/[TSS] (Fig. 6d). Means were 0.127 m^2 g^{-1} for $S \leq 5$, 0.041 m^2 g^{-1} for $7.5 \leq S \leq 15$, and 0.013 m^2 g^{-1} for $S \geq 20$.

The presence of fine particulate material passing a GF/C but retained by a 0.22 μm polycarbonate filter (Fig. 4b,c) raised the possibility that there may be fine particulate material passing a GF/F glass fiber filter (the type used for measurement of particulate absorption), but retained by a 0.22 μm membrane filter. Absorption by the particulate material caught on a 0.22 μm membrane filter after pre-filtration through a GF/F filter was measured on one sampling date, and found to vary logarithmically with CDOM absorption (Fig. 7a). The absorption by these fine particulates, which would not routinely be measured by the glass fiber filterpad method, was estimated by log–log regression as:

$$a_{\mathrm{fp}}(440) = 0.00166\left[a_g(440)\right]^{2.435} \quad (8)$$

where $a_{\mathrm{fp}}(440)$ is the absorption at 440 nm of particulate matter passing a GF/F filter but retained by a 0.22 μm membrane filter. The average spectral slope of the fine particulate material was 0.0094 nm^{-1}, similar to that for material caught on a GF/F filter during the 2003–2004 sampling period. Absorption measurements on unfiltered samples made with the ac-9 are not subject to this artifact. Comparison of $a_{t-w}(440)$ measured by the ac-9 with the sum of absorption components measured on the Cary spectrophotometer, i.e. $a_g(440) + a_\phi(440) + a_{p-\phi}(440)$, both without (Fig. 7b, filled symbols) and with (Fig. 7b open symbols) the correction calculated by Eq. (8), revealed that the calculated correction due to fine particulates has little effect on

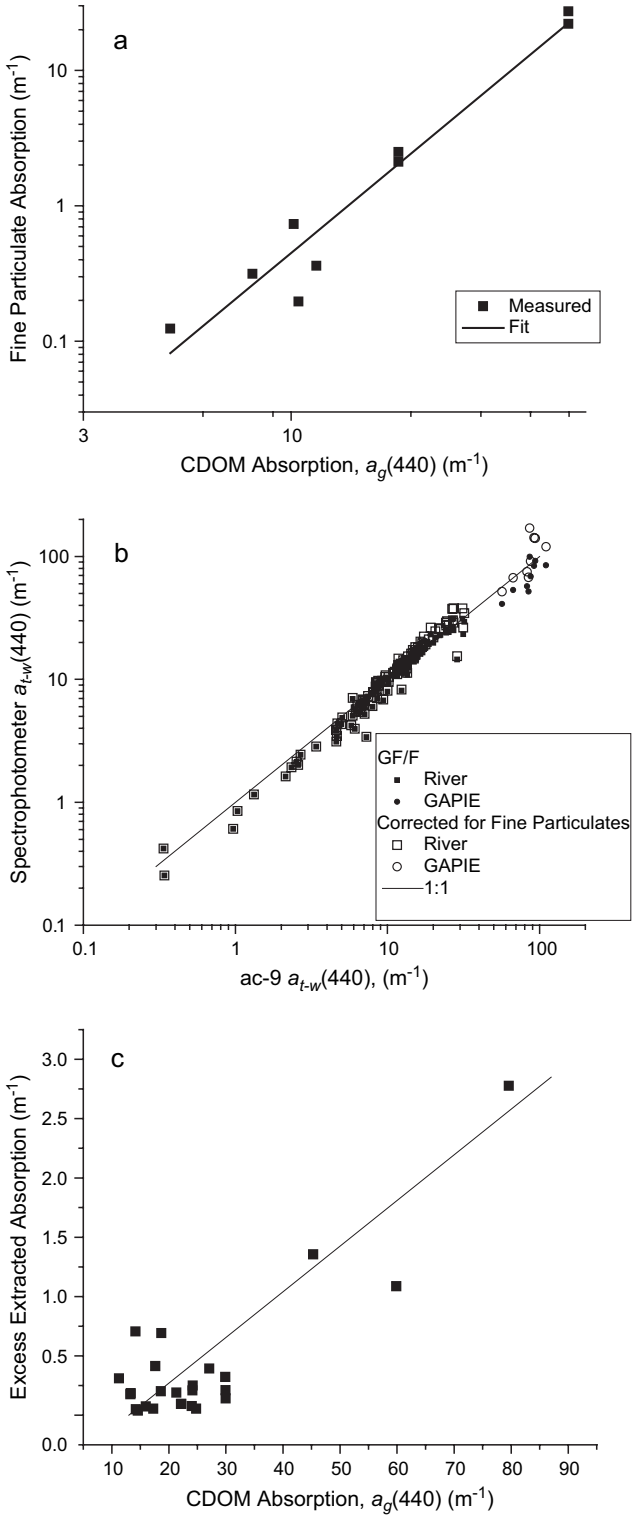

absorption estimates at $a_{t-w}(440)$ less than about $10\ m^{-1}$ (Fig. 7b). In the range $10\ m^{-1} < a_{t-w}(440) < 30\ m^{-1}$, addition of the estimated absorption by fine particulates most often resulted in overestimation of ac-9 measurements, while in samples from the Georgia Pacific impoundment effluent, correction addition of Eq. (8) to spectrophotometric absorption measurements improved agreement with ac-9 measurements in about half the samples, and resulted in overestimates in the other half (Fig. 7b).

Finally, the difficulty of estimating phytoplankton absorption when CDOM was high (Fig. 5b) suggests that some absorption by non-algal particulates may be extracted by the methanol treatment. On a subset of samples meeting the criteria CHLA $< 10\ mg\ m^3$ and CDOM $> 10\ m^{-1}$, I estimated the potential magnitude of this excess extraction as the difference between particulate absorption before and after extraction, less the expected absorption by phytoplankton, i.e., $a_p(440) - a_{extracted}(440) - a^*_\phi(440)$[CHLA]. The apparent excess extraction was positively correlated with CDOM absorption (Fig. 7c), but of smaller magnitude than the fine particulate absorption (Fig. 7a). It would appear to be more important as an interference with estimation of chlorophyll absorption than as a term in the absorption budget for the river.

5.4. Scattering

The spectral shape of scattering coefficient normalized to the observed value at 555 nm generally varied inversely with wavelength (Fig. 8a). The $b_n(\lambda)$ parameter was well fit by a power function of wavelength:

$$b_n(\lambda) = \left(\frac{555}{\lambda}\right)^n \tag{9}$$

where n is an exponent that depends on the particle-size spectrum of the particulate matter (Boss et al., 2001). While it is difficult to rule out a linear decrease with wavelength (e.g. Gould et al., 1999), the normalized scattering function appeared to flatten out at longer wavelengths (Fig. 8a), and in cases with the largest estimated n, a linear fit produced noticeably systematic errors that were improved by the power fit (Fig. 8b). The mean value of the difference $b_n(650) - b_n(715)$ was

Fig. 7. (a) Absorption by particulate matter at 440 nm that passed a GF/F glass fiber filter and was caught on a 0.22 μm membrane filter as a function of absorption by CDOM at 440 nm. (b) Sum of absorption by CDOM and particulate matter measured spectrophotometrically plotted against absorption measured with the ac-9 (filled symbols) without and (open symbols) with correction for absorption by fine particulate matter deduced from (a) (see Eq. (8)). (c) Estimated extraction of color from non-algal particulates as a function of CDOM absorption. Excess extraction was estimated as $a_p(440) - a_{extracted}(440) - a^*_\phi(440)$[CHLA] (see text).

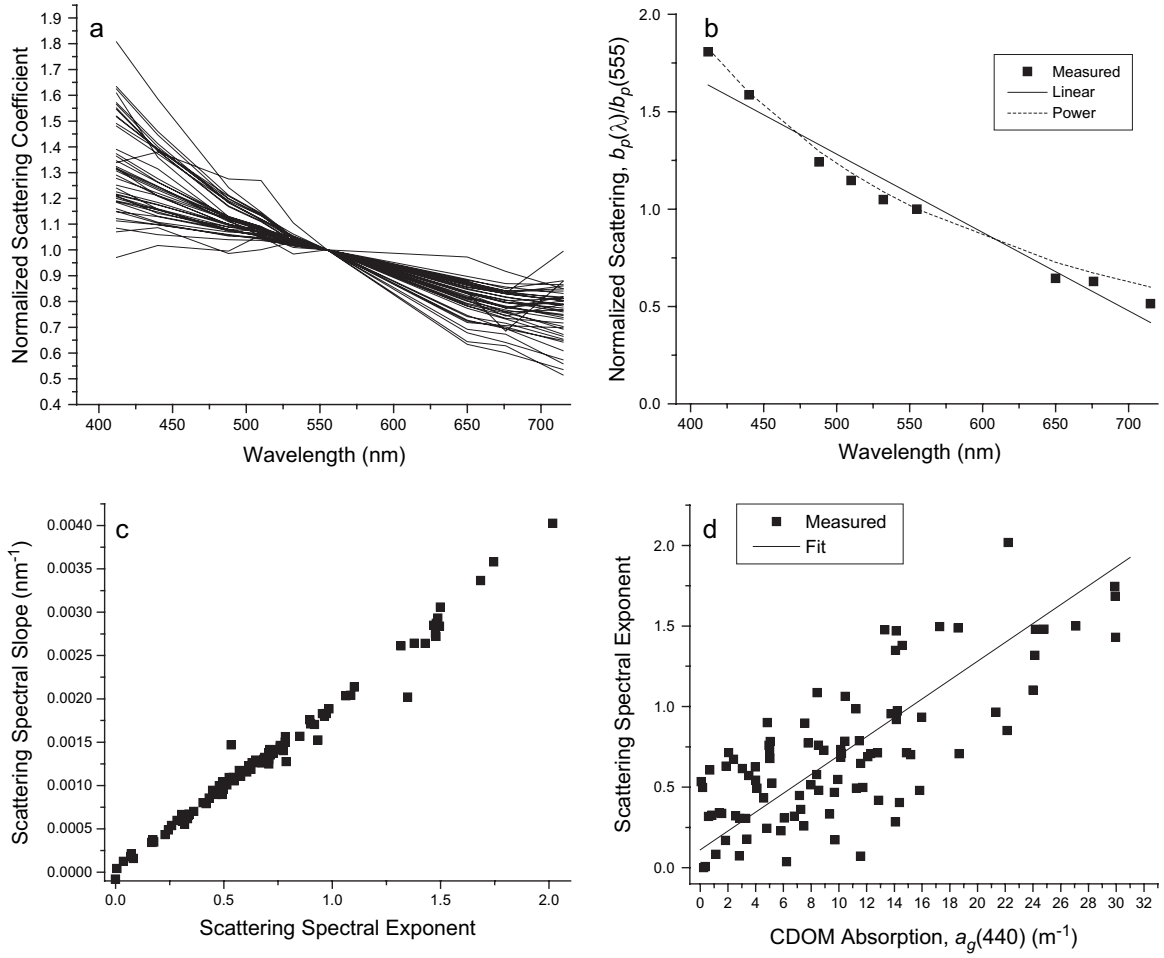

Fig. 8. (a) Normalized scattering spectra for all samples used to calculate specific-scattering coefficients. (b) Normalized scattering spectra for sample with pronounced wavelength dependence, showing fits by (solid line) linear and (dashed line) power functions. (c) Scattering spectral slope calculated by linear fit plotted against scattering spectral exponent of power function. (d) Scattering spectral exponent plotted against CDOM absorption as an indicator of the presence of fine particulate material.

significantly ($P < 0.001$) smaller than differences between comparably spaced wavelength intervals, e.g. $b_n(440) - b_n(510)$ and $b_n(488) - b_n(555)$. Indeed, there was a one-to-one correspondence between the slope estimated by linear regression and n (Fig. 8c), suggesting straightforward interconversion between linear and exponential fits. The variable n varied from 0 to 2 while the linear slope varied from 0 to $-0.004\,\mathrm{nm}^{-1}$. More importantly, n was positively correlated with CDOM absorption (Fig. 8d), consistent with the presence of fine particulate matter associated with samples with high CDOM concentrations, as determined above. Type 2 linear regression to estimate n from CDOM absorption was given by:

$$n = 0.0585 a_g(440) + 0.111 \quad r^2 = 0.56 \tag{10}$$

The relationship of the magnitude of scattering at 555 nm, $b_p(555)$, with TSS was similar to that of $a_{p-\phi}(440)$, in that different slopes were observed for samples from low (slope $= 0.609\,\mathrm{m}^2\,\mathrm{g}^{-1}$) middle (slope $= 0.236\,\mathrm{m}^2\,\mathrm{g}^{-1}$) and high salinity environments (slope $= 0.172\,\mathrm{m}^2\,\mathrm{g}^{-1}$, Fig. 9a). Additionally, both CHLA and CDOM were significant ($P < 0.001$) correlates of $b_p(555)$ in samples from low-salinity stations, whereas only TSS was a significant predictor of $b_p(555)$ at middle and high salinity stations. The following regressions were estimated as:

$$b_p(555) = 0.329[\mathrm{TSS}] + 0.124[\mathrm{CHLA}] + 0.087 a_g(440) \quad r^2 = 0.69,\ S \le 5 \tag{11a}$$

$$b_p(555) = 0.236[\mathrm{TSS}] \quad r^2 = 0,\ 7.5 \le S \le 15 \tag{11b}$$

and

$$b_p(555) = 0.173[\mathrm{TSS}] \quad r^2 = 0.45,\ S \ge 20 \tag{11c}$$

It is important to note that, while the coefficients multiplying [TSS] and [CHLA] in Eq. (11a) can be

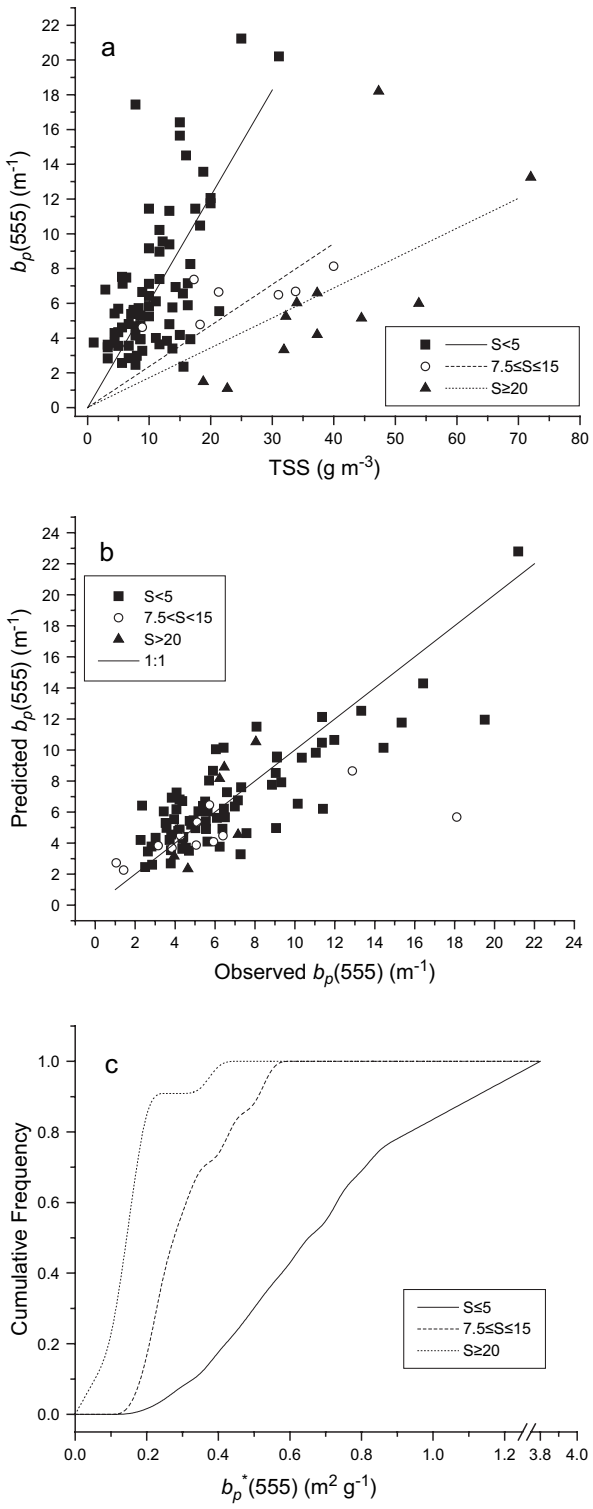

Fig. 9. (a) Scattering coefficient at 555 nm plotted against total suspended solids (TSS) for samples with salinity (S) ≤ 5 (filled squares), $7.5 \leq S \leq 15$ (open circles) and $S \geq 20$ (filled triangles). (b) Scattering coefficient at 555 nm calculated by Eqs. (11a)–(11c) plotted against observed scattering coefficient. Solid line is 1:1 line for reference. (c) Cumulative frequency distributions of specific-scattering coefficient calculated for individual samples as b_p(555)/TSS for samples with (S) ≤ 5 (solid line), $7.5 \leq S \leq 15$ (dashed line) and $S \geq 20$ (dotted line).

regarded as scattering cross-sections for those constituents, the same cannot be said for the coefficient multiplying a_g(440). That is, scattering is not attributed to the magnitude of absorption by CDOM passing through a 0.22 μm filter, but rather CDOM absorption is presumed to be correlated with a fine particulate fraction that escapes detection by measurements of TSS.

As with non-algal particulates, because of the overall degree of scatter in the relationships (indeed, Eq. (11b) was not statistically significant without an intercept), I plotted the frequency distribution of specific-scattering coefficient for individual samples estimated as b_p(555)/[TSS] (Fig. 9c). Means were $0.75\ \mathrm{m^2\ g^{-1}}$ for $S \leq 5$, $0.304\ \mathrm{m^2\ g^{-1}}$ for $7.5 \leq S \leq 15$, and $0.151\ \mathrm{m^2\ g^{-1}}$ for $S \geq 20$. Calculated in this way, the dependence of the specific-scattering coefficient on salinity interval was statistically significant ($P = 0.002$), though specific-scattering coefficients for the middle and high salinity intervals were not significantly different.

7. Discussion

In all but a few samples from the mouth of the river during the dry sampling period, CDOM was the dominant contributor to absorption coefficient integrated over visible wavelengths. Salinity was not a very good predictor of CDOM absorption (Fig. 2a,b) or of spectral slope (Fig. 3a), due to the variability in CDOM in the tidal freshwater reach of the river (Fig. 2c,d). While increases in CDOM in the downriver direction can be understood as lateral inflow from more concentrated sources (Rice Creek in the dry period, Julington Creek in the wet period, Fig. 2c,d), decreases in the downriver direction could be due to dilution by less concentrated inflow, or to photobleaching. The inverse relationship between s_g and a_g(440) suggests that photobleaching is the more likely explanation (Vodacek et al., 1997).

The values of a_g(440) measured at river stations in the LSJR (up to $30\ \mathrm{m^{-1}}$, Fig. 3c, squares) are among the highest reported for natural waters (see e.g. Table 3.2 in Kirk, 1994). It is, therefore, not surprising that CDOM absorption is the most influential optical property in a blackwater system such as the LSJR (e.g. Phlips et al., 2000). However, the effect of high CDOM concentrations went well beyond its immediate contribution to absorption. Unlike other studies of this kind (Gallegos, 1994; Gallegos and Kenworthy, 1996), here it was necessary to determine discontinuous relationships between certain inherent optical properties and water quality concentrations. For some relationships this was due to methodological problems brought on by the very high concentrations of CDOM (e.g. Eqs. (6a) and (6b)), while in others it appeared to be genuine qualitative spatial variations in optical characteristics of the particulate matter (e.g. Eqs. (11a)–(11c)).

The presence of very high concentrations of CDOM presented problems for the measurement of optical properties that can give misleading results if traditionally accepted methods are applied without scrutiny. Correlations between visually measured color in Pt units and CDOM absorption measured spectrophotometrically, which were generally linear below 200 Pt units (Fig. 4a, cf. Gallegos and Kenworthy, 1996), became nonlinear at higher visual color measurements (Fig. 4a,b). Apart from the non-linearity, some of the imprecision in Fig. 4a relates to the practice of discretizing estimates of color at 50 unit increments above 100 Pt units, evidenced by the vertically stacked points. However, the observation that filtration of both the visually and spectrophotometrically measured samples through 0.22 μm filters restored the linearity up to 800 Pt units (Fig. 4c) indicates that the non-linearity was due to fine particulate matter passing through the GF/C filter, despite a clear visual appearance. Bowling et al. (1986) and Cuthbert and del Giorgio (1992) report linearity between visual and spectrophotometric measurements up to 500 Pt units on samples filtered through 0.45 μm filters. Eqs. (6a) and (6b) are, therefore, specific to samples filtered through GF/C filters, and possibly site-specific as well. Sample preparation for the visual color estimates was time consuming when using 0.22 μm filters, and therefore is not practicable on a routine basis. For such concentrated samples, however, 1 cm cuvettes are more than adequate for spectrophotometric measurements, and require <10 ml of filtrate. The need to remove this fine particulate fraction adds to reasons already given (Cuthbert and del Giorgio, 1992) for preferring spectrophotometric measurements of CDOM absorption over visual estimates.

The practice of using 0.22 μm filters to measure CDOM absorption and GF/F filters to measure particulate absorption has always carried the possibility of missing absorption by a class of particles with diameters between 0.22 and ca. 0.7 μm. In most environments this has been considered to be small (e.g. Gallegos and Neale, 2002), due in part to the effective diameter of GF/F filters becoming smaller as particle loading increases as filtering proceeds. At concentrations of CDOM as high as those found in the St. Johns River, however, absorption by particles passing a GF/F filter and caught on a 0.22 μm filter was directly measurable (Fig. 7a), though in most samples, addition of the calculated (Eq. (8)) additional absorption did not make a large difference in total absorption (Fig. 7b). The correction for excess extraction by methanol treatment, though measurable (Fig. 8c), was deemed even smaller in its effect on estimation of NAP absorption, but was a significant artifact in determination of chlorophyll-specific absorption (Fig. 5b) in this highly colored system.

The need for separate equations in different salinity regimes to predict non-algal particulate absorption and particulate scattering from measurements of TSS can be understood in terms of physical properties of the particulate matter. The lower specific-absorption and specific-scattering coefficients for NAP at higher salinities are consistent with particulate matter dominated by silt and sand sized mineral particulates of marine origin, with higher specific-gravity than the finer, organic rich-particulates in the tidal freshwater reach (Babin et al., 2003a). The correlation of the spectral slope of scattering with CDOM absorption is further evidence that scattering at high salinities and low CDOM concentration was dominated by larger particles than at high CDOM concentrations (Fig. 8d).

The need for a term multiplying CDOM concentration to predict scattering coefficient at low salinities (Eq. (11a)) was unexpected. It is understandable, however, in light of all the other evidence (Figs. 4c, 7a) indicating the presence of a fine particulate fraction accompanying samples with high CDOM concentrations. It would, of course, be preferable on mechanistic grounds to express the effect of this particulate fraction on scattering in terms of a mass-specific scattering coefficient. Measurement of the mass concentration of that fine particulate fraction on a routine basis, however, would likely be difficult. Its close association with high CDOM concentration makes Eq. (11a) an effective operational alternative. Similarly for the spectral slope of scattering, n, CDOM concentration is a suitable correlate of the fine particulate fraction that causes inverse wavelength dependence of scattering (Fig. 8d).

8. Summary

The St. Johns River is an optically complex system in which all three optically active components contribute significantly to the total absorption and scattering spectra. In spite of the high attenuation coefficients, the tidal freshwater reach of the river supports extensive beds of *Valisneria americana* fringing the shoreline and on subtidal shoals (Brody, 1994). During dry periods when CDOM becomes reduced, phytoplankton are able to take advantage of the high nutrient concentrations derived from agricultural sources and form blooms, due to the increased availability of light within the water column (Phlips et al., 2000). There is concern among managers that the increased light attenuation from these blooms may be depriving the plant communities of what would otherwise be an important opportunity for growth. Hence there is a need to understand the effect of water quality on light propagation in this optically complex system.

Water quality monitoring data have become more prevalent in the USA since the passage of the Clean Water Act of 1977. Restoration or maintenance of water clarity is frequently one of the goals or such programs. The

procedures employed here and resulting equations provide a means of estimating the inherent optical properties from routine water quality measurements, thereby adding value to long-term, existing data on the St. Johns River. Furthermore, the scalar variables, CDOM, CHLA, and TSS are amenable to mass transport modeling, so that the equations can be used for embedding an optical model within a larger three dimensional hydrodynamic water quality model, for evaluation of the effects of management decisions on water clarity.

The accuracy with which the underwater light field can be predicted from relationships such as those presented here is fundamentally limited by the approach embodied in Eqs. (1)–(5), which combine a great variety of CDOM species and suspended particle types into a few broadly defined categories. The result of this variability is seen in the spread of the specific-absorption (Fig. 4b,d) and -scattering coefficients (Fig. 9a,c). The optical factors governing much of this variability are understood (i.e. particle-size, index of refraction, specific-gravity, Babin et al., 2003a), and indeed, progress has been made toward prediction of specific-absorption and scattering coefficients of oceanic waters from detailed knowledge of the plankton community composition (Stramski et al., 2001). The goal of future work to improve optical modeling in these complex waters should be to incorporate the needed particle and chemical measurements into field studies, and to develop the understanding needed to predict these properties from physical and biological processes.

Acknowledgements

This work was supported by contract 99B144B from the St. Johns River Water Management District. I thank J. Messer, A. Steinmetz, and M. Jeansonne for assistance in the field, and K. Yee, A. Lewis and D. Sparks for laboratory analyses.

References

Aksnes, D.L., Nejstgaard, J., Soedberg, E., Sørnes, T., 2004. Optical control of fish and zooplankton populations. Limnology and Oceanography 49, 233–238.

Babin, M., Stramski, D., 2002. Light absorption by aquatic particles in the near-infrared spectral region. Limnology and Oceanography 47, 911–915.

Babin, M., Morel, A., Fournier-Sicre, V., Fell, F., Stramski, D., 2003a. Light scattering properties of marine particles in coastal and open ocean waters as related to the particle mass concentration. Limnology and Oceanography 48, 843–859.

Babin, M., Stramski, D., Ferrari, G.M., Claustre, H., Bricaud, A., Obolensky, G., Hoepffner, N., 2003b. Variations in the light absorption coefficients of phytoplankton, nonalgal particles, and dissolved organic matter in coastal waters around Europe. Journal of Geophysical Research 108, 3211–3230.

Boss, E., Twardowski, M.S., Herring, S., 2001. Shape of the particulate beam attenuation spectrum and its inversion to obtain the shape of the particulate size distribution. Applied Optics 41, 4885–4893.

Bowling, L.C., Steane, M.S., Tyler, P.A., 1986. The spectral distribution and attenuation of underwater irradiance in Tasmanian inland waters. Freshwater Biology 16, 313–335.

Bricaud, A., Morel, A., Prieur, L., 1981. Absorption by dissolved organic matter of the sea (yellow substance) in the UV and visible domains. Limnology and Oceanography 26, 43–53.

Bricaud, A., Bédhomme, A.-L., Morel, A., 1988. Optical properties of diverse phytoplanktonic species: experimental results and theoretical interpretation. Journal of Plankton Research 10, 851–873.

Bricaud, A., Babin, M., Morel, A., Claustre, H., 1995. Variability in the chlorophyll-specific absorption coefficients of natural phytoplankton: analysis and parameterization. Journal of Geophysical Research 100, 13321–13332.

Brody, R.W., 1994. The Lower St. Johns River Basin Reconnaissance. Biological Resources, vol. 6. Technical Publication SJ94-2 St. Johns River Water Management District, Palatka, Florida.

Carder, K.L., Steward, R.G., Harvey, G.R., Ortner, P.B., 1989. Marine humic and fulvic acids: their effects on remote sensing of ocean chlorophyll. Limnology and Oceanography 34, 68–81.

Cuthbert, I.D., del Giorgio, P., 1992. Toward a standard method of measuring color in freshwater. Limnology and Oceanography 37, 1319–1326.

Davies-Colley, R.J., Vant, W.N., Smith, D.G., 1993. Colour and Clarity of Natural Waters. Ellis Horwood, Chichester.

Dennison, W.C., Orth, R.J., Moore, K.A., Stevenson, J.C., Carter, V., Kollar, S., Bergstrom, P.W., Batiuk, R.A., 1993. Assessing water quality with submersed aquatic vegetation. BioScience 43, 86–94.

Gallegos, C.L., 1994. Refining habitat requirements of submersed aquatic vegetation: role of optical models. Estuaries 17, 198–219.

Gallegos, C.L., Kenworthy, W.J., 1996. Seagrass depth limits in the Indian River Lagoon (Florida, U.S.A.): application of an optical water quality model. Estuarine, Coastal and Shelf Science 42, 267–288.

Gallegos, C.L., Neale, P.J., 2002. Partitioning spectral absorption in case 2 waters: discrimination of dissolved and particulate components. Applied Optics 41, 4220–4233.

Gould, R.W., Arnone, R.A., Martinolich, P.M., 1999. Spectral dependence of the scattering coefficient in case 1 and case 2 waters. Applied Optics 38, 2377–2383.

Jeffrey, S.W., Humphrey, G.F., 1975. New spectrophotometric equations for determining chlorophyll *a*, *b*, *c*1, and *c*2 in higher plants, algae and natural phytoplankton. Biochemie und Physiologie der Pflanzen 167, 191–194.

Kemp, W.M., Twilley, R.R., Stevenson, J.C., Boynton, W.R., Means, J.C., 1983. The decline of submerged vascular plants in upper Chesapeake Bay: summary of results concerning possible causes. Marine Technology Society Journal 17, 78–89.

Kirk, J.T.O., 1994. Light and Photosynthesis in Aquatic Ecosystems. Cambridge University Press, Cambridge.

Kishino, M., Takahashi, M., Okami, N., Ichimura, S., 1985. Estimation of the spectral absorption coefficients of phytoplankton in the sea. Bulletin of Marine Science 37, 634–642.

Mobley, C.D., Gentili, B., Gordon, H.R., Jin, Z., Kattawar, G.W., Morel, A., Reinersman, P., Stamnes, K., Stavn, R.H., 1993. Comparison of numerical models for computing underwater light fields. Applied Optics 32, 1–21.

Morris, F.W.I., 1995. The Lower St. Johns River Basin Reconnaissance. Hydrodynamics and Salinity of Surface Water, vol. 3. Technical Report SJ95-9, St. Johns River Water Management District, Palatka, Florida.

Phlips, E.J., Cichra, M., Aldridge, F.J., Jembeck, J., Hendrickson, J., Brody, R., 2000. Light availability and variations in phytoplankton standing crops in a nutrient-rich blackwater river. Limnology and Oceanography 45, 916–929.

Roesler, C.S., Perry, M.J., Carder, K.L., 1989. Modeling in situ phytoplankton absorption from total absorption spectra in productive inland marine waters. Limnology and Oceanography 34, 1510–1523.

Stramski, D., Bricaud, A., Morel, A., 2001. Modeling the inherent optical properties of the ocean based on the detailed composition of the planktonic community. Applied Optics 40, 2929–2945.

Tzortziou, M., 2004. Measurements and characterization of optical properties in the Chesapeake Bay estuarine waters using in-situ measurements, MODIS satellite observations, and radiative transfer modeling. Ph.D. dissertation, University of Maryland, College Park, Maryland.

Vodacek, A., Blough, N.V., DeGrandpre, M.D., Peltzer, E.T., Nelson, R.K., 1997. Seasonal variation of CDOM and DOC in the Middle Atlantic Bight: terrestrial inputs and photooxidation. Limnology and Oceanography 42, 674–686.

Wells, J.T., Kim, S.-Y., 1991. The relationship between beam transmission and concentration of suspended particulate material in the Neuse River estuary, North Carolina. Estuaries 14, 395–403.

Wozniak, S.B., Stramski, D., 2004. Modeling the optical properties of mineral particles suspended in seawater and their influence on ocean reflectance and chlorophyll estimation from remote sensing algorithms. Applied Optics 43, 3489–3503.